IEEE Robotics and Automation Letters (RA-L) paper, presented at ICRA 2026, Vienna, Austria. Cite as RA-L paper.

Twisted String Actuation Module for Compact Robotic Finger with Extended Stroke, Reduced Hysteresis, and Bidirectional Operation

Chunghyeon Lee, Bhivraj Suthar* and Seokhwan Jeong*, *Member, IEEE,*

***Abstract*—Twisted String Actuators (TSAs) are promising alternatives to conventional gear-based transmissions due to their high reduction ratios and compact form factors. However, practical limitations such as nonlinear hysteresis, limited stroke, and inherently unidirectional motion hinder their deployment in robotic systems. In this work, we propose a novel bidirectional TSA mechanism that addresses all three limitations simultaneously through an antagonistic configuration, asymmetric axis shift (AAS), and pre-tension tuning. This mechanism enables reliable bidirectional actuation by compensating for asymmetric contraction-extension behavior, suppresses hysteresis via adaptive tensioning, and extends the effective stroke. We implement the proposed design in a continuum finger module and derive a compact kinematic model for control. Extensive experiments validate the effectiveness of the approach, demonstrating the attenuation of the hysteresis, accurate bidirectional bending control across a wide range (±180°), and the feasibility of integration into multi-finger grippers for dexterous manipulation. The results suggest that the proposed actuator design serves as a practical and scalable solution for compact robotic systems requiring precise and reversible motion.**

***Index Terms*—Twisted string actuator, hysteresis, pre-tension, asymmetric axis shift, bidirectional, continuum finger**

I. Introduction

In many robotic actuation systems, the transmission performs a critical function by amplifying the limited torque of electric motors and matching the normal operating regions of both the motors and the robots [1]. Generally, electric motors feature a rated operating range of high speed and low torque, whereas robotic systems demand low-speed and high-torque actuation. Consequently, most transmissions consist of gear reducers with a ratio above 1:1, and various types of reducers, including planetary gears, cycloidal gears, and harmonic drives, are employed as key components in robotic actuation modules (e.g., a robotic hand often needs a ratio of at least 100:1 [2]). These reducers, however, add cost, complexity, maintenance, and impact fragility, issues that intensify as the size of the system decreases. As the trend toward smaller robotic systems accelerates, the importance of the torque amplification has grown, and research to improve reducer performance or to find alternative solutions has been actively pursued. Direct- and quasi-direct-drive schemes with larger moment arms can supply comparable torque [3]–[5], but integrating them into space-constrained, small-scale robots remains challenging.

Since the early 2010s, a twisted string actuator (TSA) [6] has emerged as a novel mechanism that can potentially replace such reducers. A TSA typically comprises one or multiple pairs of strings, converting rotational input from a motor into linear displacement through twisting of the strings. Notably, this twist-based rotation-to-linear conversion can offer extremely higher transmission ratios than that of conventional solutions [7], [8]. Moreover, TSAs can be realized relatively simply by using strings, with far less need for complex machining or costly components compared to conventional transmission systems. Due to their ease of fabrication, cost-effectiveness, and compactness, TSAs have been applied in a variety of systems such as robotic fingers [9]–[11], robotic hands [6], [12]–[14], drones [15], exoskeletons [16], [17], robotic joints [18], [19], and robotic arms [20], [21], and have been considered promising candidates for replacing conventional reducer-based transmission systems.

Despite these promising advantages, the practical application of TSAs in real robotic systems has been limited for the following reasons:

- *Twisting hysteresis* (see Fig. 1(a)): When the string has physical contact with supporting parts, uniform propagation of twisting across the entire string is disrupted, leading to hysteresis in the rotation-to-linear motion [13], [22]–[25]. Hence, any section where twisting occurs must be designed to remain free of contact, which inevitably increases the total dimension of the actuation module and further restricts the stroke.
- *Limited stroke range* (see Fig. 1(b)): Even within a contact-0 configuration, a TSA can only contract about 30% - 50% of the initial string length [13]. Beyond this range, abnormal contraction behavior called over-twisting occurs, and the rotation-to-linear relationship becomes highly nonlinear. Consequently, the feasible stroke is significantly shorter compared to other actuation mechanisms.

Manuscript received: August 6, 2025; Revised November 7, 2025; Accepted December 3, 2025.

This paper was recommended for publication by Editor Cosimo Della Santina upon evaluation of the Associate Editor and Reviewers' comments. This work was supported by the National Research Foundation of Korea(NRF) grant funded by the Korea government(MSIT)(RS-2023-00218379) and the Nano Material Technology Development Program through the NRF funded by Ministry of Science and ICT(RS-2025-25442536).

C. Lee and S. Jeong are with the Department of Mechanical Engineering, Sogang University, Seoul, South Korea (email: chee0523@gmail.com; seokhwan@sogang.ac.kr).

B. Suthar is with the School of Artificial Intelligence and Data Science, Indian Institute of Technology Jodhpur, Rajasthan, India (email: bhivraj@iitj.ac.in).

B. Suthar and S. Jeong are the corresponding authors.

Digital Object Identifier (DOI): see top of this page.

IEEE Robotics and Automation Letters (RA-L) paper, presented at ICRA 2026, Vienna, Austria. Cite as RA-L paper.

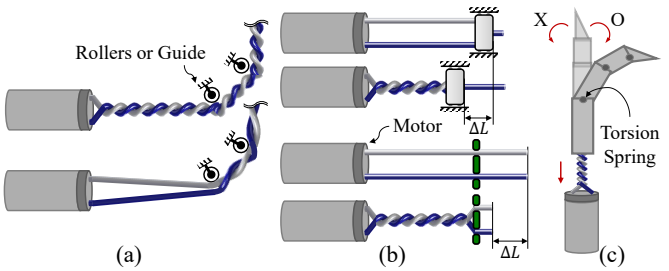

Fig. 1: Disadvantages of TSA: (a) twisting hysteresis. (b) limited stroke range. (c) unidirectional movement.

- *Unidirectional movement* (see Fig. 1(c)): Similar to general tendon-driven mechanisms, a TSA generates only contraction force, making true bidirectional actuation difficult with a single motor. Achieving bidirectional motion requires passive elements such as springs or antagonistic configurations, often involving bulky and nonlinear pulleys [18], [19].

A variety of solutions have been proposed in the TSA research community to address these challenges. Lee *et al.* and Khan *et al.* introduced bidirectional mechanisms combined with variable-radius pulleys to address the issue of unidirectional movement [18], [19]. Park *et al.* also demonstrated bidirectional motion by using multiple TSAs and pulleys driven by multiple actuators [20]. Suthar and Ryu proposed a method leveraging pre-twisting of TSAs, enabling operation within a curved conduit where physical contact occurs without hysteresis [25]. Jeong *et al.* presented guidelines for routing tendons and designing structures to extend the contraction stroke and facilitate a compact form factor suitable for integration into a robotic hand [13].

Although many TSA mechanisms have been proposed, none has yet *simultaneously* addressed three problems: (1) limited stroke range, (2) twisting hysteresis, and (3) unidirectional movement. Moreover, addressing only a part of these issues hinders the effective application of TSAs in robotic systems. In particular, the restricted stroke limits the overall form factor, negating the TSA's high transmission ratio in a compact design, and thus rendering TSA-based solutions less viable.

This paper proposes a novel TSA module, implemented in a continuum finger, that simultaneously solves the three aforementioned challenges: (1)-(3). We believe that this work will serve as a reference design framework for extending TSA-based applications, previously limited to the research stage, into real-world robotic systems.

II. Problem Analysis and Design Concept

A. Challenges in TSA-based Finger Actuation

Operating a TSA in a curved conduit or finger introduces string–surface friction, causing nonlinear hysteresis and severe performance loss. In curved passages, TSA hysteresis appears as (1) deviation between the twist and untwist trajectories; (2) incomplete return to the initial position; and (3) pullback effects [22]–[25]. TSA-related hysteresis is also apparent in a robotic finger. Fig. 2(a)–(c) illustrates the hysteresis sequence: with motor rotation angle θ, a 0 to θ_t twist contracts the string and bends the finger, while reversing to $\theta = 0$ should untwist

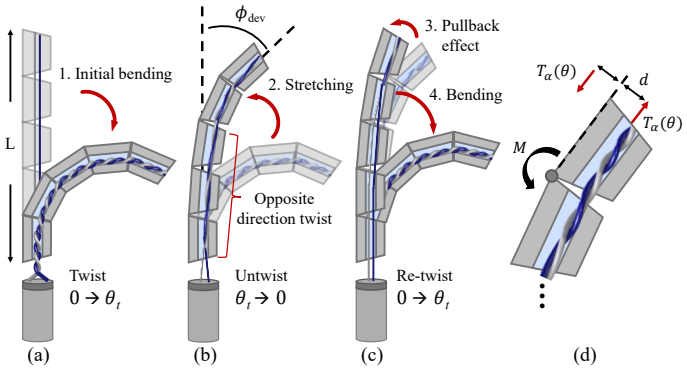

Fig. 2: Hysteresis and pullback in a TSA based robotic finger: (a) initial bending by twisting, (b) following untwist with hysteresis ϕ_{dev}, (c) re-twist causing pullback before bending. (d) Conceptual illustration of hysteresis attenuation via antagonistic tension.

the string and straighten the finger. However, during untwisting, string–channel friction lets the twist nearest the motor to untwist first; once a fully untwisted segment forms, those strands re-twist opposite to the fingertip side (see Fig. 2(b)). By the cycle's end, residual twists remain at the tip with opposite twists at the motor side, so even at $\theta = 0$ the finger stays partly bent by ϕ_{dev}. On the next twist toward θ_t, these opposite twists at the motor side untwist first, briefly extending the string and producing a slight stretch before bending begins. This undesired back-and-forth motion is known as the *pullback* effect.

Building on prior observations, we leveraged the fact that maintaining higher string tension during untwisting suppresses hysteresis. Palli *et al.* showed heavier loads or stiffer springs reduce frictional loops [22], while Suthar *et al.* reported a smaller hysteresis area under greater tension [23], [25]. Building on these insights, we sought to identify an additional tension profile that would minimize hysteresis in the finger operation. To express hysteresis, we introduce the bending angle of the finger according to the motor angle θ during twisting and untwisting sequences as $\phi_{\text{t}}(\theta)$ and $\phi_{\text{ut}}(\theta)$, respectively. The instantaneous deviation between the two trajectories ϕ_{dev} is then expressed as $\phi_{\text{dev}}(\theta) = \phi_{\text{ut}}(\theta) - \phi_{\text{t}}(\theta)$. The area formed due to this deviation is considered as a hysteresis characteristic of this system A_{hys}, given by:

$$A_{\text{hys}} = \int_0^{\theta_t} \phi_{\text{dev}}(\theta)\, d\theta = \int_0^{\theta_t} \big(\phi_{\text{ut}}(\theta) - \phi_{\text{t}}(\theta)\big)\, d\theta \qquad (1)$$

To simplify the model, we assumed that the finger is designed as a continuum structure; it can be modeled as a single elastic beam. Under this assumption, Euler–Bernoulli beam theory relates the bending angle ϕ to the string's tension through $T = M/d = EI\phi/(dL)$. By multiplying both sides of Eq. 1 by $EI/(dL)$, the expression originally written in terms of ϕ can be considered as a tension-based equation, as follows.

$$\frac{EI}{dL} A_{\text{hys}} = \frac{EI}{dL} \int_0^{\theta_t} \big(\phi_{\text{ut}}(\theta) - \phi_{\text{t}}(\theta)\big)\, d\theta = \int_0^{\theta_t} \big(T_{\text{ut}} - T_{\text{t}}\big)\, d\theta \qquad (2)$$

Here, E is the Young's modulus; I is the area moment of inertia; L is the finger length; d is the moment arm; and the string tensions during untwisting and twisting are T_{ut} and T_{t}, respectively. Assuming these material and geometric

IEEE Robotics and Automation Letters (RA-L) paper, presented at ICRA 2026, Vienna, Austria. Cite as RA-L paper.

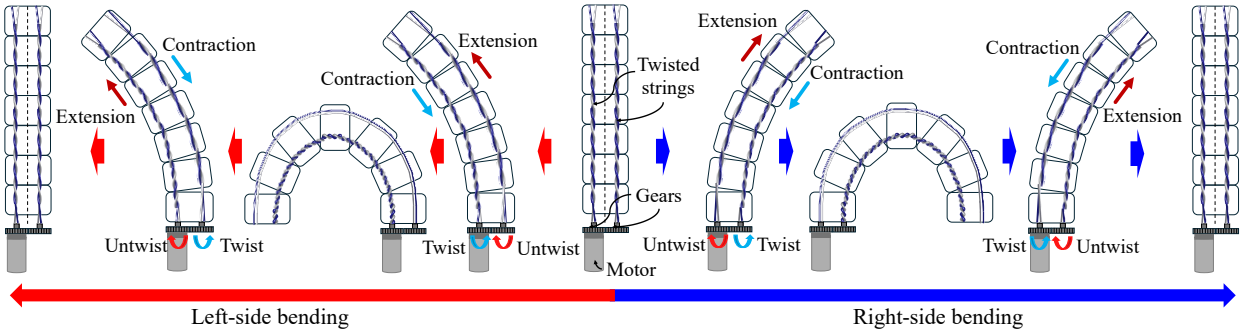

Fig. 3: Schematic of the bidirectional bending operation using the proposed TSA mechanism.

properties are constant, the term $EI/(dL)$ can be regarded as a constant C, so minimizing A_{hys} becomes equivalent to minimizing CA_{hys}. In this situation, we target to minimize CA_{hys} by applying additional antagonistic tension $T_\alpha(\theta)$ (see Fig. 2(d)). To determine the form of $T_\alpha(\theta)$, we model the reduced hysteresis area $CA^*_{\text{hys}}(T_\alpha)$ as follows.

$$\begin{aligned} CA^*_{\text{hys}}(T_\alpha(\theta)) &= \int_0^{\theta_t} \big(T_{\text{ut}}(\theta) - T_{\text{t}}(\theta)\big)\, d\theta - \int_0^{\theta_t} T_\alpha(\theta)\, d\theta \\ &= C\int_0^{\theta_t} \big(\phi_{\text{ut}}(\theta) - \phi_{\text{t}}(\theta)\big)\, d\theta - \int_0^{\theta_t} T_\alpha(\theta)\, d\theta \end{aligned} \tag{3}$$

To minimize $CA^*_{\text{hys}}(T_\alpha(\theta))$, Eq. 3 should be driven to zero, so the optimal additional tension $T^*_\alpha(\theta)$ must adopt the following form.

$$T^*_\alpha(\theta) = \arg\min_{T_\alpha(\theta)} CA^*_{\text{hys}}\big(T_\alpha(\theta)\big) \;\approx\; C\left(\phi_{\text{ut}}(\theta) - \phi_{\text{t}}(\theta)\right) \tag{4}$$

B. Proposed Bidirectional TSA Mechanism

To overcome the limitations of TSA, we introduce a bidirectional twisted-string mechanism (see Fig. 3). Eq. 4 indicates that the additional tension $T_\alpha(\theta)$ should be proportional to the deviation between the twist and untwist bending trajectories. As illustrated in Fig. 4(a), when the string untwists, the deviation increases, requiring a correspondingly larger $T_\alpha(\theta)$; this demand can be met by exploiting the contraction force of a TSA on the opposing side to function as $T_\alpha(\theta)$ (see Fig. 2(d)), leveraging its rising profile [7], [8].

To provide $T_\alpha(\theta)$ and enable true bidirectional bending simultaneously, we mount two identical TSAs in an antagonistic pair and couple them by gears (Fig. 3), so a single motor drives all of the strings. Each TSA runs through its own channel to the fingertip. Both pairs start with initial twists of same amount and direction; thus, while one untwists the other twists, producing an antagonistic action that enables bidirectional finger motion. Also, their contraction forces alternate, so the active pair supplies the additional tension, suppressing hysteresis on the untwisting side, and thus enabling one to exploit the full curved path as stroke without lengthening the actuator (see Fig. 1). Therefore, the proposed mechanism addresses the issue of '*Unidirectional movement*', '*Twisting hysteresis*', and '*Limited stroke range*' simultaneously.

However, two key challenges must be addressed to implement the proposed mechanism. First, the nonlinear behavior of the TSA, namely, the mismatch between contraction and extension *lengths* shown in Fig. 4(b)—introduces a critical asymmetry in bidirectional operation that must be compensated. Second, we need a systematic way to implement the parameter C in Eq. 4 and to determine its appropriate value that effectively reduces hysteresis. Both issues are examined in detail in Section III.

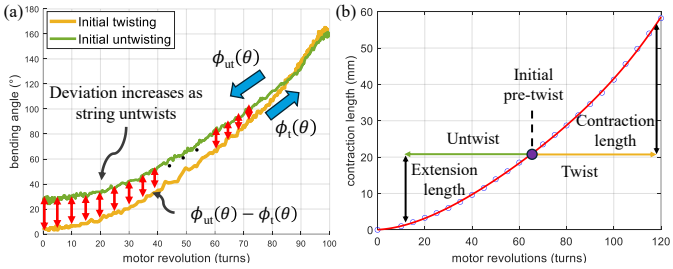

Fig. 4: (a) Bending-angle trajectories of the continuum finger: initial twisting (orange) versus the subsequent untwisting path (green). The difference $\phi_{\text{ut}}(\theta) - \phi_{\text{t}}(\theta)$ (red line) grows with motor returns to 0, illustrating the increasing deviation—and hence hysteresis—as the TSA string untwists. (b) Length difference between contraction and extension in TSA.

III. Bidirectional TSA–Continuum Finger System: Design and Control

This section aims to verify the control performance of the proposed bidirectional TSA with a continuum-type finger module. Traditional robotic fingers with 3 or 4 discrete joints are not ideal for emulating bending behaviors discussed in Section II-A. Thus, in this study, we designed a continuum finger with an elastic backbone crossing its axis.

A. Impeding Tension and Asymmetric Axis Shift

When the continuum finger is driven by a bidirectional TSA, a new problem arises. As shown in Fig. 4(b), the contraction length is always longer than the extension length, rather than satisfying the symmetry requirement for bending (i.e., contraction length = extension length). Consequently, the untwisting TSA pair provides an undesirable kinematic constraint, which generates counter tension and impedes normal bending motion. This phenomenon is defined here as *impeding tension*.

Accumulated impeding tension can over-tighten or even snap the extending string, and its excess force resists motion, degrading control accuracy. This study introduces a solution called *Asymmetric Axis Shift* (AAS), achieved by designing the finger channels with asymmetric geometry that naturally shifts the TSA axis during bending.

IEEE Robotics and Automation Letters (RA-L) paper, presented at ICRA 2026, Vienna, Austria. Cite as RA-L paper.

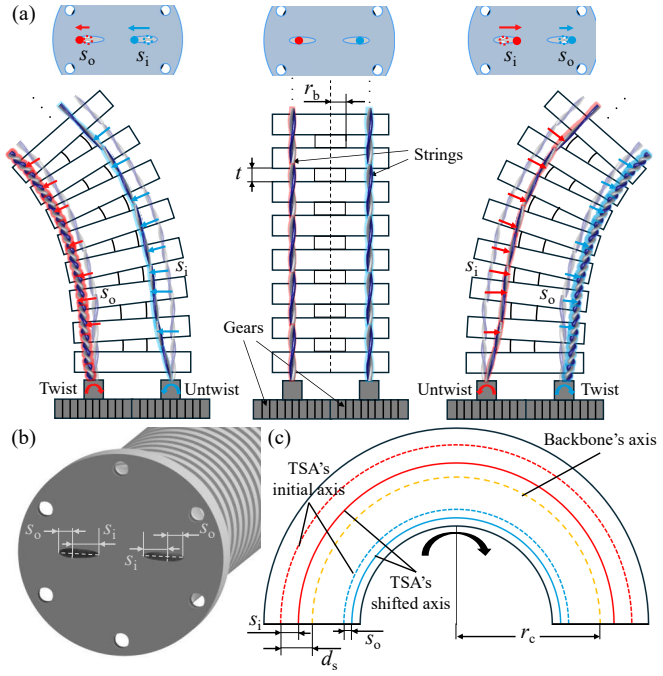

Fig. 5: (a) Schematic illustrating the operation of the AAS. (b) Channel shape of the continuum finger to induce AAS. (c) Schematic of AAS of two TSAs under 180° bending.

AAS leverages the axis-shift phenomenon: when a cable is thinner than its channel, it slides toward the finger's bending direction [26] (see Fig. 5(a)). As shown in Fig. 5(b), the two TSA channels follow ellipses with different major axes, giving inner and outer shifts s_i and s_o. Fig. 5(c) depicts the worst-case 180° bend with the radius of the bending curvature r_c, where impeding tension is maximized. Here d_s is the distance from the backbone axis to the initial TSA axis, r_b is the radius of the backbone, and t is the notch spacing. Given these parameters, the required contraction and extension lengths (i.e., the difference between the TSA length at the initial axis when the finger is first stretched and the TSA length at the shifted axis when the finger is bent) X_{cont}, X_{ext} can be described by:

$$X_{\text{cont}} = \pi r_c - \pi\big(r_c - (d_s + s_o)\big) - 2\left(\sqrt{s_o^2 + t^2} - t\right) \quad (5)$$

$$X_{\text{ext}} = \pi\big(r_c + (d_s - s_i)\big) + 2\left(\sqrt{s_i^2 + t^2} - t\right) - \pi r_c \quad (6)$$

To eliminate impeding tension through the AAS, the condition $d_s - r_b > s_i > s_o$ must be satisfied. Under the condition $s_i > s_o$, the axis of the untwisting TSA shifts more than that of the twisting TSA during bending, thereby satisfying the required contraction and extension lengths without generating impeding tension. The condition $d_s - r_b > s_i$ ensures that the design is physically realizable—that is, the channels do not cut into the backbone. The square root terms in Eq. 5 and 6 account for the fixed TSA ends, where the string is shifted diagonally. With two equations, one inequality, and five parameters (d_s, r_b, s_i, s_o, t), the channel shape can be designed to compensate for the impeding tension at the maximum bending angle. For instance, to fully leverage the TSA's nonlinear stroke, a larger s_i can be selected to allow a wider extension margin, while tuning d_s and s_o to maintain the desired module size.

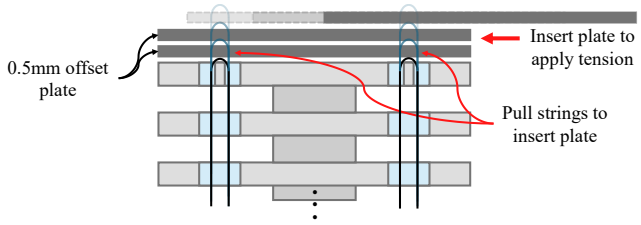

Fig. 6: Schematic illustrating the pre-tension method: thin offset plates (0.5 mm each) are inserted between the string loops at the fingertip, shifting the anchor position and thereby adding tension to the TSA strings in the finger module.

B. Pre-tension Tuning

This section deals with implementing the parameter C in Eq. 4 and selecting its appropriate value. Our strategy is to regulate the antagonistic tension by pre-loading both pairs of TSA strings with an equal *pre-tension* while the finger is in its neutral (straight) state. A higher pre-tension increases the contraction force produced during subsequent bending and stretching.

To introduce pre-tension, we insert thin offset plates at the fingertip, between the two TSA loops (see Fig. 6). Both pairs of TSAs are connected identically to match the dimensions of the designed finger module and actuator. Introducing the plate shifts the anchor position of the TSA pairs upward, which stretches the string and incrementally increases their tension. By varying the number of plates, we experimentally determine the minimum pre-tension that suppresses hysteresis and pullback; this measured value is then used to define the parameter C indirectly.

C. Design of Bidirectional TSA Module

This section presents the detailed design of the proposed bidirectional TSA, configured in an *antagonistic* structure with the combined continuum finger module. We adopt a single-motor design that drives two meshed gears simultaneously. Fig. 7(a) presents an exploded view of the actuation module: the motor gear is rigidly attached to the motor shaft, whereas the opposing gear rotates on a bearing. To achieve symmetric bidirectional motion, the gears are set to a 1:1 ratio. A connector frame links the finger module to the motor bracket, and thrust bearings mounted at the front of both gears inside the frame effectively compensate for the large axial contraction forces of the TSA pairs. Two sets of TSAs are fixed to the respective gears, routed through the finger's internal channels, and anchored to a pre-tension plate at the fingertip. Fig. 7(b) shows the configuration of the fully assembled system. Fig. 7(c) illustrates the side view operation of the bidirectional TSA. When the motor rotates, one TSA pair contracts while the other extends, bending the finger toward the twisting side. Reversing the rotation bends it oppositely, enabling fully bidirectional motion.

D. Design Process

This section details a step-by-step design framework for the bidirectional TSA and its continuum finger module. Fig. 8

IEEE Robotics and Automation Letters (RA-L) paper, presented at ICRA 2026, Vienna, Austria. Cite as RA-L paper.

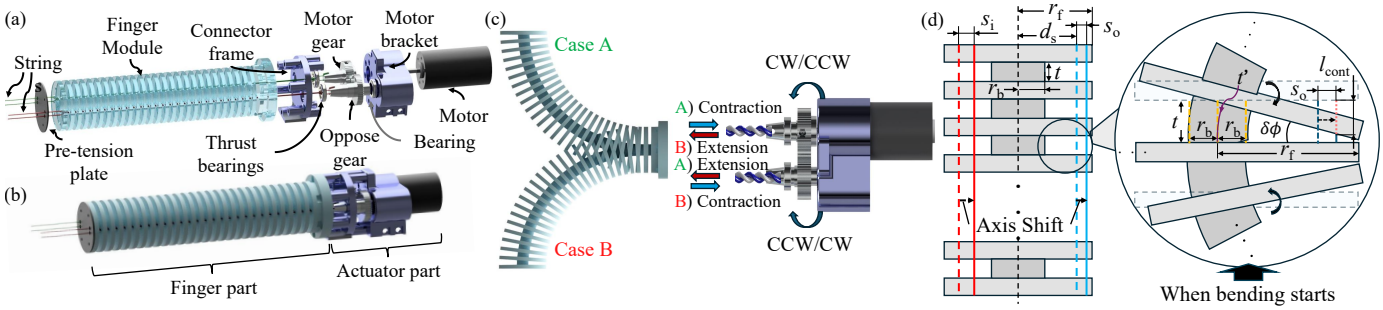

Fig. 7: Detailed design of the continuum finger with bidirectional TSA module- (a) Exploded view, (b) Assembled view, (c) Upper view schematic about how motor and gear rotation determines the direction of bending. (d) Schematic of the continuum finger's bending process and its parameters.

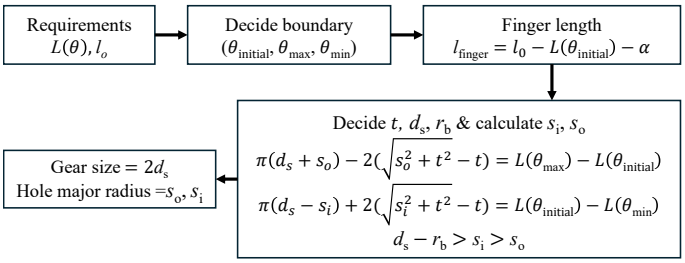

Fig. 8: Flow chart of the design process to decide parameters.

outlines the design process, allowing designers set the target stroke and select structural parameters.

Typically, the theoretical estimation of the TSA's contraction length l_c is given by the following equation [22]:

$$l_c = \sqrt{l_0^2 \left(1 + \frac{F_i}{K}\right)^2 - \theta^2 r^2} \tag{7}$$

where l_0 is the initial length of the string, F_i is the applied tension, K is the stiffness coefficient of the string, θ is the motor rotation, and r is the radius of the twisted string. While this equation reasonably generalizes TSA kinematics, its accuracy is limited in practical application, showing errors up to 27.88% [8].

To address this, we employed an empirical model $L(\theta)$ that directly approximates the contraction length as a function of θ. The plot shown in Fig. 4(b) was measured using Dyneema string (#1.5, $\varnothing 0.2, 12.2\,\text{kg}$ maximum load) with the initial string length set to $l_0 = 170\,\text{mm}$. The string was twisted in 5-turn increments, and actual contraction lengths were measured with a linear encoder (YS20-100-01-C, Wuxi Yansen). With the measured data points, a 4th-order polynomial $L(\theta)$ with minimum RMSE was fitted.

Returning to Fig. 8, we next determine the motor rotation range: the initial twist angle (θ_{initial}) and max/min angle bound (θ_{max} and θ_{min}). The bound is determined within the nominal twisting range, avoiding over-twisting [27]. Setting θ_{initial} at the midpoint of the allowable range maximizes the feasible stroke. In this study, we used $\theta_{\text{initial}} = 65$, $\theta_{\text{max}} = 120$, and $\theta_{\text{min}} = 15$, covering a total range from 15 to 120 turns.

Once θ_{initial} is set, the length of the finger is determined by subtracting the contraction length at θ_{initial} from l_0, and also subtracting the physical distance α between the channel entrance and the string's fixed point. If the connector frame (see Fig. 7(a)) is designed thin enough, α is negligible, allowing twist–untwist to begin right at the channel entrance.

Next, based on the target finger size, the designer selects values for t, d_s, and r_b and solves for s_o and s_i using the Eq. 5 and 6, with the constraint $d_s - r_b > s_i > s_o$. Here, select the backbone radius r_b as small as practicable while still supporting the finger to minimize torque loss during bending. Finally, based on the calculated values, the gear dimensions and AAS channel profile are determined.

E. Control Method

This section describes the kinematic model to achieve the desired bending angle of the underactuated continuum finger embedding TSA, based on Fig. 7(d) and Table I.

First, consider the contact between two adjacent notches in Fig. 7(d). As bending starts, the backbone forms a curved shape, so the originally straight segment of length t follows an arc of length t'. Because the bending angle per notch $\delta\phi$ is small, this arc can be approximated by its chord (i.e., $t' \approx t$). Under this approximation, the unit bending angle satisfies:

$$\delta\phi = \frac{t}{r_f}. \tag{8}$$

As illustrated in Fig. 7(d), l_{cont} is required when the string shifts and bends by $\delta\phi$. This value can be calculated as:

$$l_{\text{cont}} = t - \left(r_f - d_s - s_o\right) \tan(\delta\phi) \tag{9}$$

Assuming that the same amount of bending angle $\delta\phi$ occurs in every notches, the total bending angle is the sum of these individual angles. Consequently, the contraction length required to bend the finger to the target angle ϕ_t is given by:

$$l_{\text{d.cont}} = N \cdot l_{\text{cont}} = \frac{\phi_t}{\delta\phi} \cdot \left(t - \left(r_f - d_s - s_o\right) \tan(\delta\phi)\right) \tag{10}$$

Next, using the $L(\theta)$ introduced in Section III-C, the required motor turns θ_{motor} to achieve $l_{\text{d.cont}}$ is given by:

$$\theta_{\text{motor}} = L^{-1}\left(\frac{\phi_t}{\delta\phi} \cdot \left(t - \left(r_f - d_s - s_o\right) \tan(\delta\phi)\right)\right) \tag{11}$$

IV. Experiment Results

A. Hardware Configuration and Experiment Setup

A prototype (see Fig. 9(a)) was fabricated with the parameter values listed in Table I to validate the bidirectional TSA module and continuum finger designed in Section III. Close-up views of the parts explained in Section III are shown in

IEEE Robotics and Automation Letters (RA-L) paper, presented at ICRA 2026, Vienna, Austria. Cite as RA-L paper.

TABLE I: Nomenclature and its specifications

Name	Meaning	Value
r_f	Radius of the finger	16 mm
d_s	Distance between string and axis	9.5 mm
s_i	Length of string's inner axis shift	5.3 mm
s_o	Length of string's outer axis shift	3.1 mm
$\delta\phi$	Bending angle per notch	8.9°
ϕ_t	Target bending angle	(-180°, 180°)
N	Number of required bending notches to reach desired angle	$\phi_t/\delta\phi$
r_b	Radius of the backbone	4 mm
t	Distance between two notches	2.5 mm
l_{cont}	Contraction length per unit node	1.87 mm
$l_{\text{d.cont}}$	Desired total contraction length to bend ϕ_t	$N \times 1.87$ mm

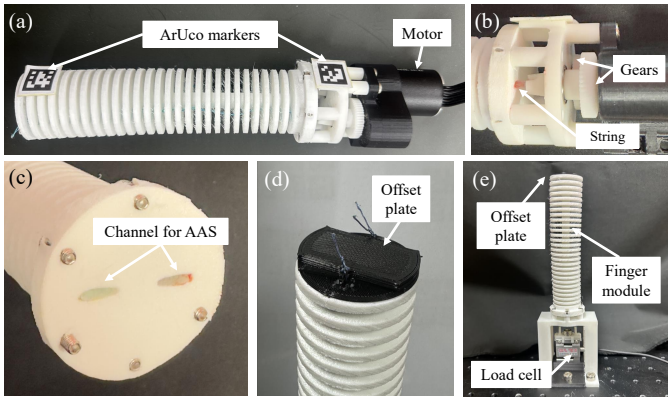

Fig. 9: (a) Prototype of the bidirectional TSA-continuum finger with ArUco marker attached. Close view of (b) actuator part, (c) channel for AAS, (d) offset plate. (e) Experiment setup to measure the magnitude of pre-tension.

Fig. 9(b)–(d). Fig. 9(e) shows the load-cell setup (DBCM-50 kg, BONGSHIN) used to measure pre-tension. The actuator module is driven in direct-drive manner without a gear amplification by a brushless DC motor (BL2446S, Motorbank) and controlled with ESCON 70/10 4-Q Servo controller (Maxon Motor). Both gears and the actuator parts were 3D-printed (White Resin V5, Form 4 Formlabs), providing high strength and fine resolution. The continuum finger was 3D-printed with a flexible Thermoplastic Polyurethane filament (TPU 95A, Moment M300), offering the flexibility and moment capacity required for large bending angles. To minimize friction, the inner surfaces of the finger channels were coated with polytetrafluoroethylene spray. Each TSA is equipped with a 170 mm long Dyneema string identical to the one described in Section III-D. Two ArUco markers were attached to the outer surface of the finger to enable real-time vision-based measurement of the bending angle. The system was controlled by a microcontroller (LAUNCHXL-F28379D, Texas Instruments) through the C2000 microcontroller blockset in MATLAB Simulink (R2022b), with a sampling frequency of 200 Hz.

B. Experiment Result of Pre-tension

The measured pre-tension values were then tested under actual operating conditions (both TSA strings initially twisted 65 turns and actuated ±55 turns repeatedly) to observe the hysteresis during bending-stretching. Fig. 10 and Table II present the results of the continuum finger with different offset

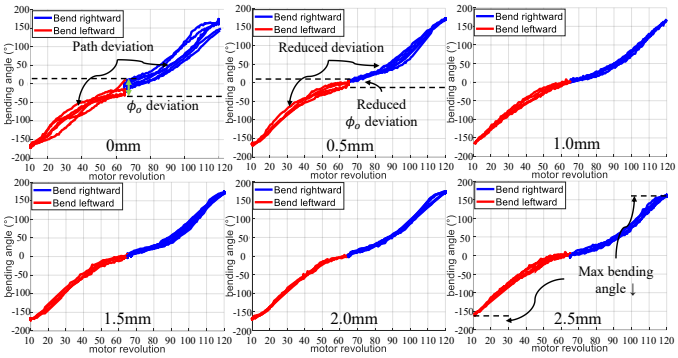

Fig. 10: Result of controlling continuum finger using bidirectional TSA with various pre-tension offsets (0mm, 0.5mm, 1mm, 1.5mm, 2mm, 2.5mm).

plate thicknesses from 0 mm to 3.0 mm. In Table II, the A_{hys} denotes the average hysteresis area per cycle.

With no pre-tension (e.g., 0 mm offset), the twist–untwist trajectories diverge widely, showing large hysteresis and leaving the finger offset from its initial position. Adding a 0.5 mm offset reduces the hysteresis area A_{hys} and deviation, yet some persists, indicating that the pre-tension is insufficient. Offsets of 1–2 mm provide enough pre-tension to effectively attenuate hysteresis—the finger consistently returns to its initial position and the control trajectory remains highly repeatable across successive cycles without any noticeable deviations. At 2.5 mm, the extra pre-tension starts to cut the available bending range and reintroduces impeding tension that hinders motion. Applying the offset to 3 mm overloads the string, which leads to string snaps during bending.

In summary, an offset of 1–2 mm eliminates hysteresis in the proposed system, while excessive offsets degrade control and overstress the string, risking snap; this finding provides an indirect guideline for implementing the constant C in Eq. 4.

TABLE II: Effect of Pre-tension (Mean±Standard deviation)

Offset	$T_{\text{pre}}(N)$	$A_{\text{hys}}(\text{rad}^2)$	ϕ_o deviation (°)	$\phi_{\max}$ reduction(°)	Snap
0 mm	0	15.04±1.52	23±0.91	n	×
0.5 mm	0.5±0.04	4.77±0.86	9±0.96	n	×
1 mm	1.1±0.07	1.79±0.41	n	n	×
1.5 mm	1.6±0.06	1.48±0.16	n	n	×
2 mm	2.1±0.09	1.51±0.12	n	n	×
2.5 mm	2.8±0.06	1.86±0.36	n	9±0.89	×
3 mm	3.2±0.08	u	u	20±1.12 (before snap)	○

n: negligible ($< 2.5°$), u: unknown, ○: snap observed, ×: no snap

C. Control Results of Continuum Finger Module

Using the Eq. 11 kinematics, we commanded eight bend targets—$\pm45°, \pm90°, \pm135°$, and $\pm180°$—which correspond to motor rotations of $\pm18, \pm32, \pm43$, and ±53 turns, respectively. The bending angles were monitored in real time with an ArUco-based vision system, and the pre-tension offset was fixed at 1.5 mm for all trials.

Fig. 11(a) illustrates the motion of the finger bending and returning to the initial state during a sequence of twist–untwist–untwist–twist commands: all eight targets bend and recover with negligible hysteresis and no pullback. From $\pm45°$ to $\pm180°$, measurements closely track model-based motor commands. Fig. 11(b)–(c) compares the desired bending angles and the experimental results, and shows an average error of 6.7%. This stems from elastic deformation and modeling

IEEE Robotics and Automation Letters (RA-L) paper, presented at ICRA 2026, Vienna, Austria. Cite as RA-L paper.

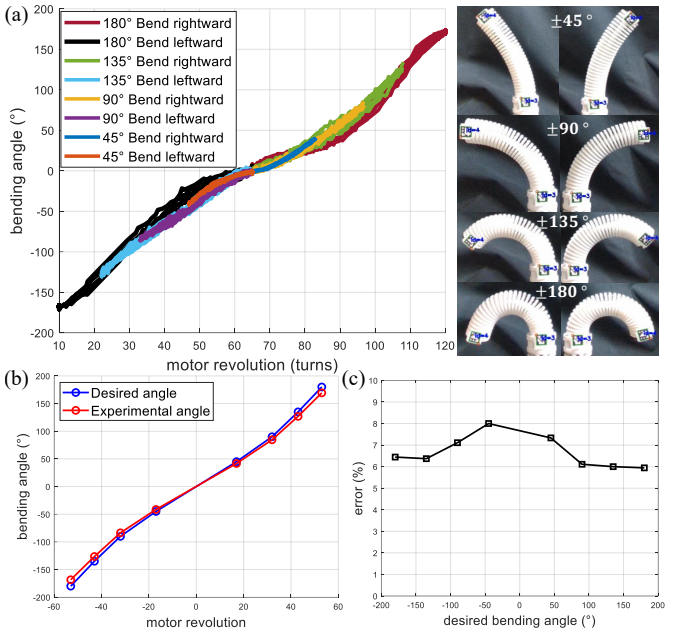

Fig. 11: (a) Bending angle control of the continuum finger with bidirectional TSA. (b) Comparison of desired and experimental angles. (c) Error between desired and experimental angles.

simplifications in the kinematics (ideal notch contact, axis-shift approximation) that slightly under-predict required turns. The angle difference increases with bending angle, yet Fig. 11(c) shows the largest error(%) at $\pm 45°$, where the string first slides (axis shifts) before starting to bend the finger. Even so, the average error across all eight targets was $7.1°$, confirming the control method's practical validity.

D. Hysteresis: Bidirectional TSA vs Unidirectional TSA

With the same experimental setup, we compared the hysteresis behavior of a conventional unidirectional TSA (single pair) with that of the proposed bidirectional TSA under repeated twist-untwist cycles. Fig. 12(a)-(c) shows the corresponding trajectories, and the results are summarized in Table III.

With the unidirectional TSA (see Fig. 12(a)), the finger failed to return to its initial position, exhibiting ϕ_o deviation of approximately $21°$ and a pullback of $9°$. The mismatch between the twisting and untwisting curves produced a hysteresis loop. In contrast, when the bidirectional TSA was operated in the left- and right-bending modes (see Fig. 12(b), (c)), ϕ_o deviation was reduced to $5°$ and $4°$, respectively, which is about 80% reduction, and no pullback was observed in either direction. Because the twist and untwist trajectories nearly overlapped, the hysteresis loop also disappeared.

These results imply that the proposed bidirectional TSA markedly attenuates hysteresis, increases stroke, and provides bidirectional motion with a compact form factor.

TABLE III: Comparison between conventional and bidirectional TSA

	Conventional TSA	**Bi-TSA (Right)**	**Bi-TSA (Left)**
ϕ_o deviation	$21°$	$5°$	$4°$
Pullback	$9°$	$<< 1°$	$<< 1°$
Hysteresis loop	○	×	×

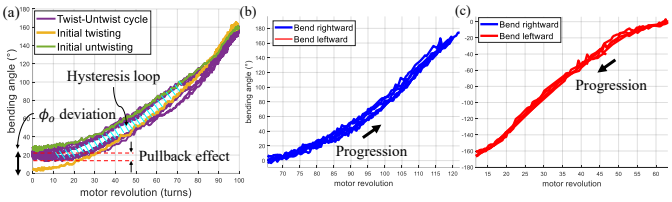

Fig. 12: TSA operation results: (a) unidirectional; (b) bidirectional, rightward bending; (c) bidirectional, leftward bending.

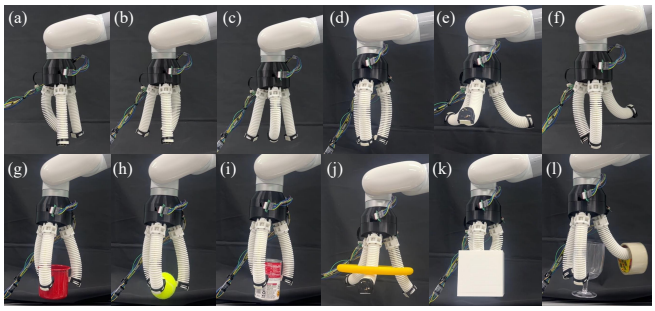

Fig. 13: Dexterous actions of bidirectional TSA gripper: (a)-(c) independent bending, (d) inward grasping, (e) outward grasping, (f) bidirectional grasping, (g)-(i) demonstrations of inward grasping, (j)-(k) demonstrations of outward grasping, (l) demonstration of bidirectional grasping.

E. Additional Performance Evaluation

Quantitative tests were conducted to evaluate mechanical performance. The tip force increased from 3.57 N at 45° to 9.82 N at 180°, confirming the TSA's high transmission ratio. Efficiency peaked at 77.3% under 500 g and dropped to 66.1% under 1000 g, showing optimal performance under moderate loads. In the payload test (100 g, 200 g, 500 g, 1000 g), the finger maintained its posture for 60 seconds without deformation. The repeatability test over 30 cycles showed deviations below 2° across all eight bending angles, with only minor variations among them. Durability tests revealed creep and pre-tension degradation after about 3000 cycles. The related contents are shown in the supplementary video.

F. Application to Gripper

This section evaluates a three-finger gripper actuated by the proposed TSA mechanism to demonstrate the effectiveness of the approach. Conventional robotic fingers typically employ a unidirectional tendon-driven design, which limits their ability to actively utilize the opposing direction. In contrast, the proposed bidirectional mechanism enables multi-directional bending and diverse in-hand manipulations, thereby enhancing spatial efficiency in manipulation tasks.

Fig. 13(a)–(c) illustrate dexterous gripper motions where each finger independently performs bidirectional actuation. Fig. 13(d), (g)–(i) show inward bending for conventional grasping, while Fig. 13(e), (j)–(k) demonstrate outward bending that enables reaching into hollow objects (e.g., boxes) for internal grasping of ring-shaped or partially enclosed items. This ability to individually direct the action of each finger enables a variety of dexterous and adaptive manipulation strategies.

IEEE Robotics and Automation Letters (RA-L) paper, presented at ICRA 2026, Vienna, Austria. Cite as RA-L paper.

V. Discussion and Conclusion

This study proposed a TSA design framework that simultaneously achieves bidirectional bending, suppresses pullback, and attenuates the hysteresis that plagues existing TSA applications. With a calibrated pre-tension, the finger consistently returned to its initial position, reducing the origin angle deviation 21° to $4^\circ - 5^\circ$ (i.e., 80% reduction) and removing the 9° pullback seen in the conventional configuration. The kinematic model shows average tracking errors of 6.7%.

The current system still presents several limitations. The durability, which is defined as reliable actuation lifetime, is approximately 3000 cycles, after which creep and pre-tension degradation become apparent. This can be mitigated by applying pre-stress treatment to the string and more precisely manufactured AAS geometry that completely eliminates residual impeding tension, thereby improving fatigue resistance and extending operational reliability. The kinematic model, though compact and practical, assumes uniform notch contact and rigid segments, which constrains prediction accuracy at large bending angles. Considering variable curvature and elastic coupling between adjacent notches may improve its fidelity in future implementations. In addition, the offset-plate pre-tensioning method, while simple and repeatable, requires re-identification of appropriate values whenever design parameters change. As part of our future work, we plan to develop a simple yet adaptive pre-tensioning method that retains quantitative control of the offset-plate approach while improving adaptability to varying load and configuration conditions.

Currently, the system operates under open-loop control, and future research will focus on integrating bending or tension sensors to enable real-time feedback and closed-loop angle control for enhanced precision. Beyond the current gripper example, the antagonistic TSA concept can be scaled to wearable exosuits, continuum arms, and other compact robotic systems, broadening the reach of bidirectional, high-stroke actuation mechanisms.

References

[1] J. Park, J. Lee, H.-T. Seo, and S. Jeong, "Variable transmission mechanisms for robotic applications: A review," *IEEE Robotics & Automation Magazine*, 2024.

[2] J. T. Belter, J. L. Segil, A. M. Dollar, R. F. Weir *et al.*, "Mechanical design and performance specifications of anthropomorphic prosthetic hands: a review," *J. Rehabil. Res. Dev*, vol. 50, no. 5, pp. 599–618, 2013.

[3] A. Bhatia, A. M. Johnson, and M. T. Mason, "Direct drive hands: Force-motion transparency in gripper design," in *Robotics: science and systems*, 2019.

[4] P. M. Wensing, A. Wang, S. Seok, D. Otten, J. Lang, and S. Kim, "Proprioceptive actuator design in the mit cheetah: Impact mitigation and high-bandwidth physical interaction for dynamic legged robots," *Ieee transactions on robotics*, vol. 33, no. 3, pp. 509–522, 2017.

[5] J. Seiler, N. Schêfer, G. Zhao, B. Latsch, M. Grimmer, P. Beckerle, and M. Kupnik, "Human-exoskeleton interaction force estimation based on quasi-direct drive actuators," in *2024 10th IEEE RAS/EMBS International Conference for Biomedical Robotics and Biomechatronics (BioRob)*. IEEE, 2024, pp. 1132–1139.

[6] G. Palli, G. Borghesan, and C. Melchiorri, "Modeling, identification, and control of tendon-based actuation systems," *IEEE Transactions on Robotics*, vol. 28, no. 2, pp. 277–290, 2011.

[7] G. Palli, C. Natale, C. May, C. Melchiorri, and T. Würtz, "Modeling and control of the twisted string actuation system," *IEEE/ASME Transactions on Mechatronics*, vol. 18, no. 2, pp. 664–673, 2013.

[8] I. Gaponov, D. Popov, and J. Ryu, "Twisted string actuation systems: A study of the mathematical model and a comparison of twisted strings," *IEEE/ASME Transactions on Mechatronics*, vol. 19, no. 4, pp. 1331–1342, 2014.

[9] Y. J. Shin, H. J. Lee, K.-S. Kim, and S. Kim, "A robot finger design using a dual-mode twisting mechanism to achieve high-speed motion and large grasping force," *IEEE Transactions on Robotics*, vol. 28, no. 6, pp. 1398–1405, 2012.

[10] S. H. Jeong, K.-S. Kim, and S. Kim, "Development of a robotic finger with an active dual-mode twisting actuation and a miniature tendon tension sensor," in *2016 IEEE International Conference on Advanced Intelligent Mechatronics (AIM)*. IEEE, 2016, pp. 1–6.

[11] B. Suthar, M. I. Awad, L. Seneviratne, Y. Zweiri, and I. Hussain, "Design of robotic finger using twisted string actuator with modular passive return rotational joints to achieve high grasping force: Application to wearable sixth finger," *Mechatronics*, vol. 99, p. 103157, 2024.

[12] S. H. Jeong, K.-S. Kim, and S. Kim, "Designing anthropomorphic robot hand with active dual-mode twisted string actuation mechanism and tiny tension sensors," *IEEE Robotics and Automation Letters*, vol. 2, no. 3, pp. 1571–1578, 2017.

[13] S. Jeong, Y. Lee, and K.-S. Kim, "Applications: Twisted string actuation-based compact automatic transmission," in *2021 IEEE International Conference on Robotics and Automation (ICRA)*. IEEE, 2021, pp. 10 870–10 876.

[14] R. Konda, D. Bombara, S. Swanbeck, and J. Zhang, "Anthropomorphic twisted string-actuated soft robotic gripper with tendon-based stiffening," *IEEE Transactions on Robotics*, vol. 39, no. 2, pp. 1178–1195, 2022.

[15] B. Suthar and S. Jung, "Design and feasibility analysis of a foldable robot arm for drones using a twisted string actuator: Frad-tsa," *IEEE Robotics and Automation Letters*, vol. 6, no. 3, pp. 5769–5775, 2021.

[16] P. Tran, S. Jeong, and J. P. Desai, "Voice-controlled flexible exotendon (flexotendon) glove for hand rehabilitation," in *2019 IEEE/RSJ International Conference on Intelligent Robots and Systems (IROS)*. IEEE, 2019, pp. 4834–4839.

[17] M. Dragusanu, D. Troisi, B. Suthar, I. Hussain, D. Prattichizzo, and M. Malvezzi, "Mglove-ts: A modular soft glove based on twisted string actuators and flexible structures," *Mechatronics*, vol. 98, p. 103141, 2024.

[18] D. Lee, D. H. Kim, C. H. Che, J. B. In, and D. Shin, "Highly durable bidirectional joint with twisted string actuators and variable radius pulley," *IEEE/ASME Transactions on Mechatronics*, vol. 25, no. 1, pp. 360–370, 2019.

[19] M. A. Khan, B. Suthar, I. Gaponov, and J.-H. Ryu, "Single-motor-based bidirectional twisted string actuation with variable radius pulleys," *IEEE Robotics and Automation Letters*, vol. 4, no. 4, pp. 3735–3741, 2019.

[20] J. Park, J.-i. Park, H.-T. Seo, Y. Liu, K.-S. Kim, and S. Kim, "Control of tendon-driven (twisted-string actuator) robotic joint with adaptive variable-radius pulley," in *2020 20th International Conference on Control, Automation and Systems (ICCAS)*. IEEE, 2020, pp. 1096–1098.

[21] B. Hasanen, B. Suthar, Y. Zweiri, L. Seneviratne, and I. Hussain, "Design of twisted string actuated flexure joint for supernumerary robotic arm for bi-manual tasks," *IEEE Sensors Journal*, 2024.

[22] G. Palli, M. Hosseini, and C. Melchiorri, "Twisted string actuation with sliding surfaces," in *2016 IEEE/RSJ International Conference on Intelligent Robots and Systems (IROS)*. IEEE, 2016, pp. 260–265.

[23] B. Suthar, M. Usman, H. Seong, I. Gaponov, and J.-H. Ryu, "Preliminary study of twisted string actuation through a conduit toward soft and wearable actuation," in *2018 IEEE International Conference on Robotics and Automation (ICRA)*. IEEE, 2018, pp. 1234–1239.

[24] J.-H. Ryu, I. Gaponov, and B. Suthar, "Effect of vibration on twisted string actuation through conduit at high bending angles," in *2019 IEEE/RSJ International Conference on Intelligent Robots and Systems (IROS)*. IEEE, 2019, pp. 1234–1239.

[25] B. Suthar and J. H. Ryu, "Twisted string actuation through a conduit: Undesirable behaviors and pre-twist effects," *Mechatronics*, vol. 96, p. 103084, 2023. [Online]. Available: https://www.sciencedirect.com/science/article/pii/S095741582300140X

[26] J. Kim, S.-i. Kwon, Y. Moon, and K. Kim, "Cable-movable rolling joint to expand workspace under high external load in a hyper-redundant manipulator," *IEEE/ASME Transactions on Mechatronics*, vol. 27, no. 1, pp. 501–512, 2022.

[27] M. Tavakoli, R. Batista, and P. Neto, "A compact two-phase twisted string actuation system: Modeling and validation," *Mechanism and Machine Theory*, vol. 101, pp. 23–35, 2016.